

# Search of spin-dependent fifth forces with precision magnetometry

N. Crescini,<sup>1,2,\*</sup> G. Carugno,<sup>2,3</sup> P. Falferi,<sup>4</sup> A. Ortolan,<sup>1</sup> G. Ruoso,<sup>1</sup> and C.C. Speake<sup>5</sup>

<sup>1</sup>*INFN-Laboratori Nazionali di Legnaro, Viale dell'Università 2, 35020 Legnaro (PD), Italy*

<sup>2</sup>*DFA - Università degli Studi di Padova, Via Marzolo 8, 35131 Padova, Italy*

<sup>3</sup>*INFN-Sezione di Padova, Via Marzolo 8, 35131 Padova, Italy*

<sup>4</sup>*INFN-CNR, Fondazione Bruno Kessler, and INFN-TIFPA, Via alla Cascata 56, 38123 Povo (TN), Italy*

<sup>5</sup>*School of Physics and Astronomy, University of Birmingham, West Midlands B15 2TT, UK*

Spin-dependent fifth-forces are associated with particles beyond the standard model. In particular, light pseudo-scalar bosons mediate long-range forces, allowing mass to interact with spins. The search of these interactions can be performed by periodically varying the distance between a source mass and a spin ensemble, in order to modulate the force intensity and detect it with precision magnetometry techniques. In our setup the force arises from room temperature lead masses and is detected in a paramagnetic crystal at 4.2 K, whose magnetisation is monitored by a SQUID-based magnetometer with the sensitivity of  $53 \text{ aT}/\sqrt{\text{Hz}}$ . Our measurement places the most stringent constraints on a spin-mass interaction in the ranges 1 cm to 10 m and 10 km to 300 km, improving existing limits up to more than two orders of magnitude. We show that this experimental technique may be further leveraged to explore a vast region of the fifth force's parameter space, with an interaction range longer than a few centimetres.

## I. INTRODUCTION

The known fundamental forces of nature are four: electromagnetism, weak interaction, strong interaction, and gravity. The standard model of particle physics is a remarkably successful theory that unifies the first three, and explains the forces as the exchange of the respective gauge bosons, i.e. photons,  $Z^0$  and  $W^\pm$ , and gluons [1, 2]. Grand unification theories, like string theory, also describe the gravitational interaction as mediated by a graviton [3, 4]. Strong and weak interactions are called short-range forces, since they act in a typical length below  $10^{-15} \text{ m} = 1 \text{ fm}$ , the size of a nucleus, while electromagnetic and gravitational interactions have infinite range. The mass of the mediator  $m$  determines the force range through the Compton wavelength

$$\lambda = \frac{h}{mc}, \quad (1)$$

where  $h$  is the Planck constant and  $c$  is the speed of light in vacuum. The  $Z^0$  and  $W^\pm$  bosons are heavy, so the weak interaction strength rapidly decreases approximately above 0.001 fm. All the other gauge bosons are massless and mediate long-range forces, with the peculiarity of the strong interaction, being effectively short-ranged because of color confinement. Gravity and electromagnetism do not allow for the coupling between spin and mass in the absence of relative motion, implying that a long-range spin-mass force is necessarily a fifth force, not encompassed by the standard model.

The existence of ultralight scalar particles is conjectured by a number of theories beyond the standard model, usually as a consequence of the Nambu-Goldstone

theorem [5]. Among these particles the axion is particularly well-motivated, since it arises from the Peccei and Quinn solution of the strong CP problem [6, 7], and is of cosmological interest as an acknowledged Dark Matter candidate [8]. Axions, together with axion-like particles (ALPs), are the subject of a wide and flourishing research, which in the last years encountered a conspicuous expansion [9, 10]. Along with particle physics, the search of ALP mediated forces is strongly motivated by astrophysics, as at long distances they may, for example, affect structure formation or even overwhelm gravity [8, 10]. The search of new macroscopic forces as a way to detect ALPs was first suggested by Moody and Wilczek [11], and triggered a number of experimental efforts [12–24]. These are framed in the so called “pure laboratory” searches, as they do not rely on any source of force outside the experiment itself, and consist of low-energy precision measurements assessing anomalies of present theories. In the plethora of exotic interactions, three different potentials arise from the exchange of a spin-0 boson [31, 32]: dipole-dipole, monopole-dipole, and monopole-monopole. Hereafter we focus on the description of monopole-dipole interactions, which macroscopically can be viewed as spin-mass forces; for the case of an electron ( $e^-$ ) nucleon ( $N$ ) interaction an example Feynman diagram is shown in Fig. 1a.

Despite seemingly compelling arguments for exotic phenomena [25], presently, there is no evidence of a new force of nature. The most stringent limits are essentially obtained with torsion balances [15, 16, 18–21], comagnetometers [14, 24] and magnetic materials coupled to SQUIDs [12, 17, 22], or likewise with other experimental techniques which have been proposed [26–28] or already applied [13, 23]. Moreover, the analysis of combined pure laboratory and astrophysical limits [29], and the study of atomic and molecular electric dipole moments [30] gave outstanding results in toughening the bounds on monopole-dipole interactions. Pure laboratory searches

\*Present address: IBM Research-Zürich, Säumerstrasse 4, CH-8803 Rüschlikon, Switzerland; Electronic address: ncr@zurich.ibm.com

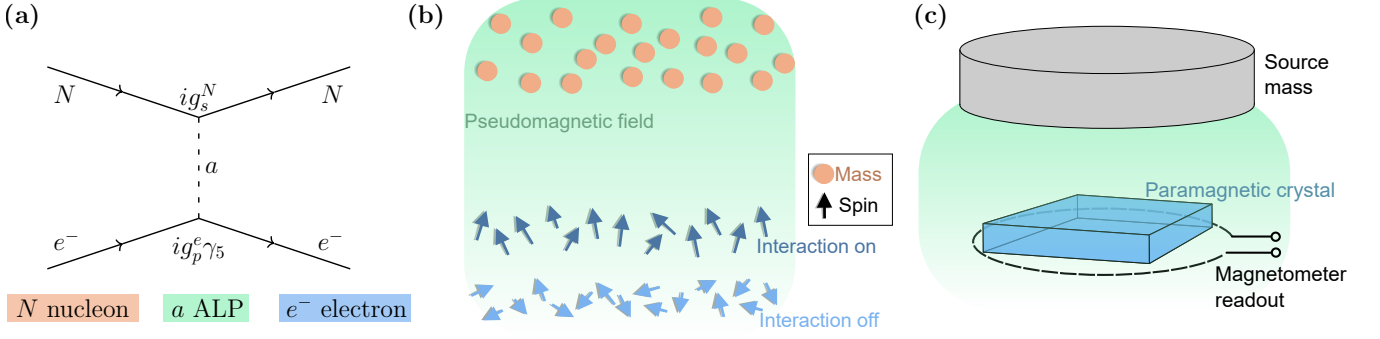


FIG. 1: Feynman diagram, particle description, and schematic drawing of the experiment. (a) The diagram represents the interaction between a nucleus  $N$  and the spin of an electron  $e^-$ , mediated by an ALP  $a$  whose scalar nucleon coupling is  $g_s^N$  and pseudoscalar electron one is  $g_p^e$ . (b) The pink circles are the nuclear masses generating the pseudomagnetic field attracting the spins, which are dark blue (light blue) arrows for  $r \ll \lambda$  ( $r \gg \lambda$ ). (c) A lead block (grey) hosts the monopole masses, and the paramagnetic crystal (blue) is the spin detector. The drawing is not to scale, see text for further details.

of fifth forces remain of absolute importance for the understanding of fundamental physics, and, with this work, we indicate a scheme which drastically improves present experimental constraints, and has the potential to overcome astrophysical bounds.

The use of a magnetic material as a detector of spin-dependent forces was pioneered by Vorobyov and Gitarts [12], followed by Ni and collaborators [17], who held the best limits on this type of interaction for more than a decade. More recently, a measurement by our group [22] improved these constraints with a pilot setup, which demonstrated the effectiveness of our experimental configuration. In this work we further develop the apparatus, obtain much improved results, and hence demonstrate the extraordinary sensitivity that can be attained by searching for fifth forces with precision magnetometry. Below, we show how a larger size apparatus may evade the main fundamental noises of the scheme, allowing the exploration of a much wider range of the monopole-dipole parameter space.

## II. FIFTH FORCE SIGNAL

The non-relativistic monopole-dipole interaction related to the Yukawa couplings in the diagram of Fig. 1a reads

$$V(\mathbf{r}) = \frac{\hbar^2 g_p^e g_s^N}{8\pi m_e} \hat{\sigma} \cdot \hat{\mathbf{r}} \left( \frac{1}{\lambda r} + \frac{1}{r^2} \right) e^{-r/\lambda}, \quad (2)$$

where  $\hbar = h/2\pi$ ,  $g_p^e$  and  $g_s^N$  are the pseudoscalar and scalar couplings of the ALP to electrons and nucleons,  $m_e$  is the electron mass and  $\hat{\sigma}$  is its Pauli vector, and  $\mathbf{r} = r \hat{\mathbf{r}}$  is the spatial vector connecting the nucleon to the spin. The potential violates parity and time-reversal and hence it is not CP conserving. Eq. (2) states that for  $r < \lambda$  the minimum energy configuration is the spin pointing towards the mass, condition which is exponentially relaxed when  $r > \lambda$ , as shown in Fig. 1b. In this

sense, using the Bohr magneton  $\mu_B$ , the potential may be recast as a pseudomagnetic field acting on an electron spin  $V(\mathbf{r}) = -\mu_B \hat{\sigma} \cdot \mathbf{b}(\mathbf{r})$ , yielding

$$\mathbf{b}(\mathbf{r}) = -\frac{\hbar g_p^e g_s^N}{4\pi q} \hat{\mathbf{r}} \left( \frac{1}{\lambda r} + \frac{1}{r^2} \right) e^{-r/\lambda}, \quad (3)$$

where  $q$  is the charge of the electron. The field  $\mathbf{b}(\mathbf{r})$  is not mediated by photons, so it does not respect Maxwell's equations, and is not screened by superconducting shields, allowing us to place the detector in a magnetically controlled environment without reducing the interaction intensity. Moreover, we can take advantage of its polynomial and exponential dependence on  $r$  to modulate the interaction strength, and thus the searched for signal, by varying the spin-mass distance (see Fig. 1b).

A typical apparatus to probe the pseudomagnetic field  $\mathbf{b}(\mathbf{r})$  is formed by an ensemble of nuclei in a macroscopic mass, called source, and a collection of spins composing the detector. To calculate the pseudomagnetic field generated by the source mass, one needs to integrate Eq. (3) over its volume  $\Omega$ . Assuming a uniform nuclear density  $\varrho_n$ , the field at the detector position results

$$B_p = \varrho_n \int_{\Omega} \mathbf{b}(\mathbf{r}) d\Omega, \quad (4)$$

whose integration can be performed by numerical or analytical means [17, 22, 23]. Microscopically, the field  $B_p$  effectively tilts the spins in the direction of the mass, so macroscopically it changes the detector's magnetisation [33], which can be detected with a magnetometer, as displayed in Fig. 1c. In this sense the magnetic material turns a pseudomagnetic field into a real one through its magnetic susceptibility  $\chi$ , and the arising signal is

$$\mu_0 M = \chi B_p, \quad (5)$$

which, for simplicity, is expressed in units of Tesla using the magnetic permeability of vacuum  $\mu_0$ .

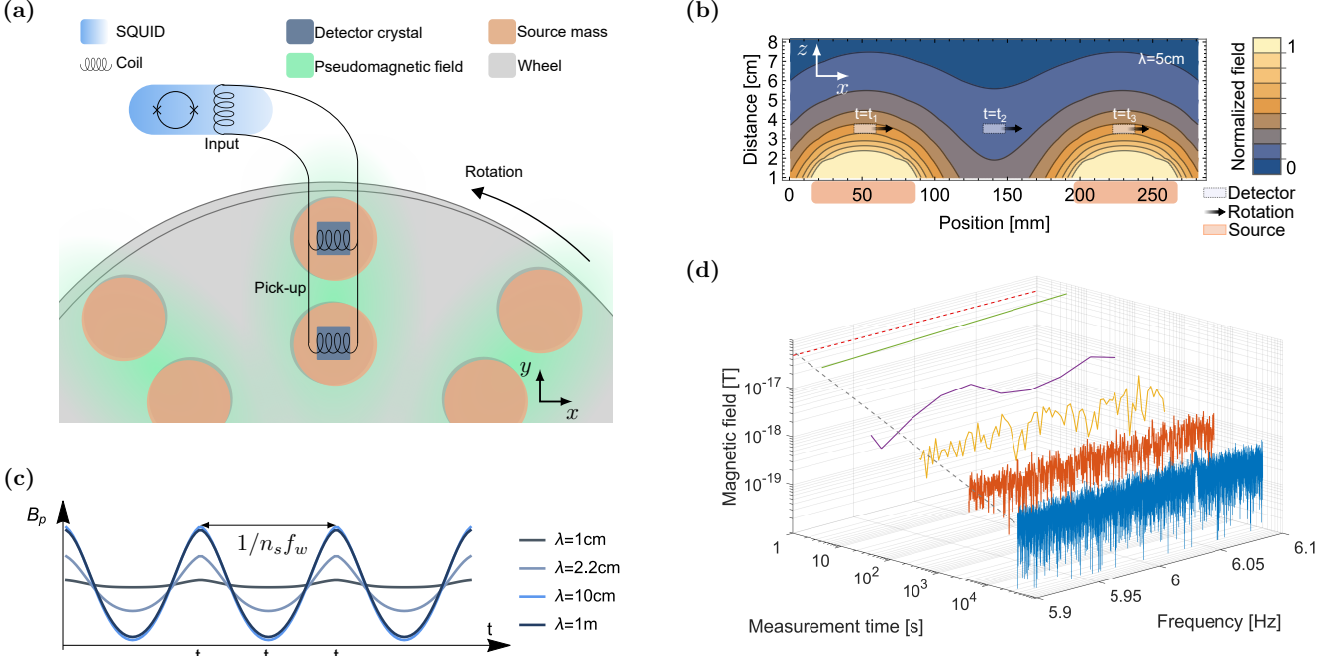


FIG. 2: Signal modelling and integrated magnetic background. (a) Scheme of the experimental apparatus (not to scale). The paramagnetic crystals (dark blue), the pick-up superconducting coils, and the SQUID are at liquid helium temperature. The room temperature part of the setup are the lead masses (orange) fixed to the wheel (grey), which, when rotating, modulate the source-detector distance (see the Methods sections for more details). (b) Contour plot of the pseudomagnetic field generated by two neighbouring source masses, where the rectangles show the detector and source positioning. At the times  $t_1$  and  $t_3$  the signal is maximum, while at  $t_2$  it is minimum. (c) Time dependence of the pseudomagnetic field for different Compton wavelengths. Different tones of blue show the signal modulation due to some example wavelengths, which are calculated with the numerical integration of Eq.(4). The times  $t_{1,2,3}$  correspond to those of the previous figure. (d) Solid lines are the magnetic field spectra in the frequency band of the signal for integration times ranging from 4 s (green) to 11 h (blue). The grey dashed line shows the  $1/\sqrt{t}$  trend of the noise, which is respected throughout the entire measurement, and the red dashed line is the SQUID background estimation.

### III. EXPERIMENTAL SETUP

As the magnetic sensitivity is a key element for this type of searches, we feature in our apparatus a SQUID-based magnetometer, which is among the most sensitive sensors available. State-of-the-art SQUIDs are affected by a flux noise of about  $1 \mu\phi_0/\sqrt{\text{Hz}}$ , where  $\phi_0 \simeq 2 \times 10^{-15} \text{ Wb}$  is a flux quanta. It is well known [34] that a SQUID magnetometer can be configured to optimize the field sensitivity over the spatial resolution, as was established by J.E. Zimmerman [34, 35] and is presently used in different fundamental and applied physics experiments [36–38]. This improvement is effective as long as the searched for field is distributed over the whole pick-up coil area. In our case, this means that the magnetometer coils have to be filled with the magnetic sample, while the  $B_p$  monopole source must be provided by sizeable masses.

The magnetic samples used as detectors are two paramagnetic  $\text{Gd}_2\text{SiO}_5$  (GSO) crystals [39] with a magnetic susceptibility  $\chi \simeq 0.7$  [40], and dimensions  $2.5 \times 2.5 \times 1.1 \text{ cm}^3$ . The GSO crystals fill two superconducting pick-up coils wired to a SQUID as shown in Fig. 2a. The two

inductances are connected in parallel, to match the input impedance of the SQUID and maximise the magnetic field sensitivity of the magnetometer [34]. The overall system calibration relies on the measurement of the flux-to-voltage conversion coefficient of the SQUID sensor, and on the calculation of the field-to-flux transduction of the pick-up coils. See Fig. 2a for the circuit scheme and the Methods Section for further details. The source producing the ALPs signal consists of  $n_s = 12$  pairs of masses mounted on an aluminum disk of about 1 m diameter. The total 24 masses are lead cylinders of 6 cm height and 5 cm diameter, whose nucleon density is  $\rho_n \simeq 6.8 \times 10^{30} \text{ m}^{-3}$ . The pairs are evenly spaced over the disk circumference, and each of the masses composing the pair is mounted on the same radius, as depicted in Fig. 2a. A rotation of the resulting wheel at a frequency  $f_w$  varies the source-detector distance with a frequency  $n_s f_w$ . An oscillating  $B_p$  periodically orients the spins toward the masses, resulting in a modulation of the GSO's magnetisation detected by the SQUID. The component of the SQUID spectrum at the frequency  $n_s f_w$  could thus contain the pseudomagnetic field signal. The source of this setup is at room temperature, while de-

tector is placed in a controlled environment, namely, a liquid helium cryostat at a temperature of 4.2 K. The cryostat is enclosed in two  $\mu$ -metal shields, while the detector is surrounded by two additional layers of superconducting NbSn shields. We achieved a minimum source-detector distance of 3.5 cm between the GSO's centre of mass and the lead cylinders surface. The pseudomagnetic field is unaffected by the layers screening the electromagnetic radiation, allowing us to model its amplitude ignoring them, as is reported in Fig. 2b. Numerically solving Eq. (4) in the case of our experimental configuration, we obtain the shape and amplitude of the expected signal generated by the wheel rotation, as shown in Fig. 2c.

The wheel rotation is driven by a brushless motor synchronous with a function generator, guaranteeing a stable and persistent signal. We use a capacitive sensor to monitor the sources rotation, and verify that its frequency does not change more than 20 parts per million in more than ten hours of measurement, assuring a coherent integration time which exceeds the run time determined by the cold time of the cryostat.

A significant advantage of this approach lies in the control of the signal frequency, which allows us to operate the setup where the magnetic noise is favourable and, as lower bound, matches the one of the SQUID. We choose to work at a sweet spot at  $n_s f_w \simeq 6$  Hz by rotating the wheel at  $f_w \simeq 0.5$  Hz, at this frequency the magnetic field noise of the SQUID-based magnetometer reaches the value of  $53 \text{ aT}/\sqrt{\text{Hz}}$ , as shown in the spectra of Fig. 2d. Within the uncertainties, this background is compatible with our estimation, primarily consisting of the SQUID noise, and with a smaller contribution likely due to the crystals' magnetisation noise. The reader is referred to the Methods section for a detailed noise budget. We leverage the fact that the pseudomagnetic signal frequency is stable within  $1/t$ , the measurement duration, to keep narrowing the measurement bandwidth and hence reduce the noise as  $\sqrt{t}$ . From the plots in Figs. 3a, 3b and 3c, which are collected simultaneously, one can see that the magnetic spectra approach a white and constant noise in a frequency band close to  $n_s f_w$ , and is entirely compatible with stochastic fluctuations at the pseudomagnetic field frequency, evidenced in Figs. 3a and 3b. The integrated signal and background of the run are reported in Figs. 3d and 3e. As demonstrated by the spectra of Fig. 2d, the noise respects this decreasing trend at least for an integration time of  $4.1 \times 10^4$  s, consistently with a zero-mean gaussian fluctuation, like thermal noise. In about 11 hours, the minimum persistent field detectable by our magnetometer with a unity signal-to-noise ratio results  $0.26 \text{ aT}$ .

#### IV. FIFTH FORCE SEARCH

This magnetic measurement was performed while the source wheel of the setup was rotating, as shown in Fig. 3c, so it can be translated into a limit on the oscillat-

ing pseudomagnetic field generated by the lead masses. The pursued signal would manifest itself as a sharp one-bin spike of precisely controlled frequency, which should be visible above the white noise of the setup, as shown in the integrated spectra of Fig. 3d and 3e. We use the waveform obtained with Eq. (5), and shown in Fig. 3d, to estimate the minimum pseudomagnetic field detectable with our measurement, and the related monopole-dipole coupling strength. So far experimental searches are mainly reporting limits on  $g_p^e g_s^N$ , but in principle both electrons and nucleons in the source masses are monopolar sources. Since our scheme is also sensitive to the electron-electron coupling  $g_p^e g_s^e$  [30], the corresponding limit is reported in Fig. 4. In lead the number of nucleons is  $A = 2.5 Z$ . The number of electrons is thus 2.5 times less than the number of nucleons, and we scale the respective signal accordingly. Our result is consistent with pure white noise and no signal compatible with a spin-mass interaction has been detected, the corresponding  $2\sigma$  upper limit on the coupling constants is  $g_p^e g_s^N \leq 4.1 \times 10^{-32}$  and  $g_p^e g_s^e \leq 1.1 \times 10^{-31}$  for  $\lambda \gtrsim 10 \text{ cm}$  at 95% confidence level. The limit for the full range of  $\lambda$  is presented in Fig. 4, where it is also compared with previous results on this type of interaction.

This work places the most stringent upper bounds on spin-mass interactions over orders of magnitude in the force range  $\lambda$ , or equivalently in the ALP mediator mass  $m$ . Between 1 cm and 1 m we advance our previous result [22] and the limit obtained with a  $^3\text{He}$ -K comagnetometer [24] of roughly two orders of magnitude. Above 1 m and below 10 m we improve the result of a torsion pendulum [19] whose monopole source is the Earth, which exceeds our measurement's sensitivity above 10 m. For Compton wavelengths of more than 10 km the latter experiment, due to the possible presence of systematic uncertainties, does not provide constraints, and the limit was set by stored-ion spectroscopy [13]. The present work improves this limit up to range of about 300 km. We do not further discuss the ranges  $\lambda \leq 1 \text{ cm}$  and  $\lambda \geq 10^3 \text{ km}$ , but mention that torsion balances [19, 21] provide the best limits. We note that, although the sensitivity reached in this work lies seven orders of magnitude away from the model-predicted value of the  $g_p^e g_s^N$  coupling [10], we believe that further significant improvements to the experimental method can be made.

First we consider direct improvements of the present setup. The employment of a *LC* pick-up coil [41, 42] on resonance with the signal would enable us to eliminate the SQUID background and to be limited by the magnetisation noise. On the other hand, the resonant circuit needs a quality factor such that its Johnson noise does not exceed the SQUID noise [43], which at low frequencies becomes a challenging technical problem. Crystals with a much higher  $\chi$  may significantly improve the experimental sensitivity by raising the signal, however, such materials usually have a much higher magnetisation noise. A simpler solution to enhance the setup is to use a quantum-limited SQUID [41] to minimize its



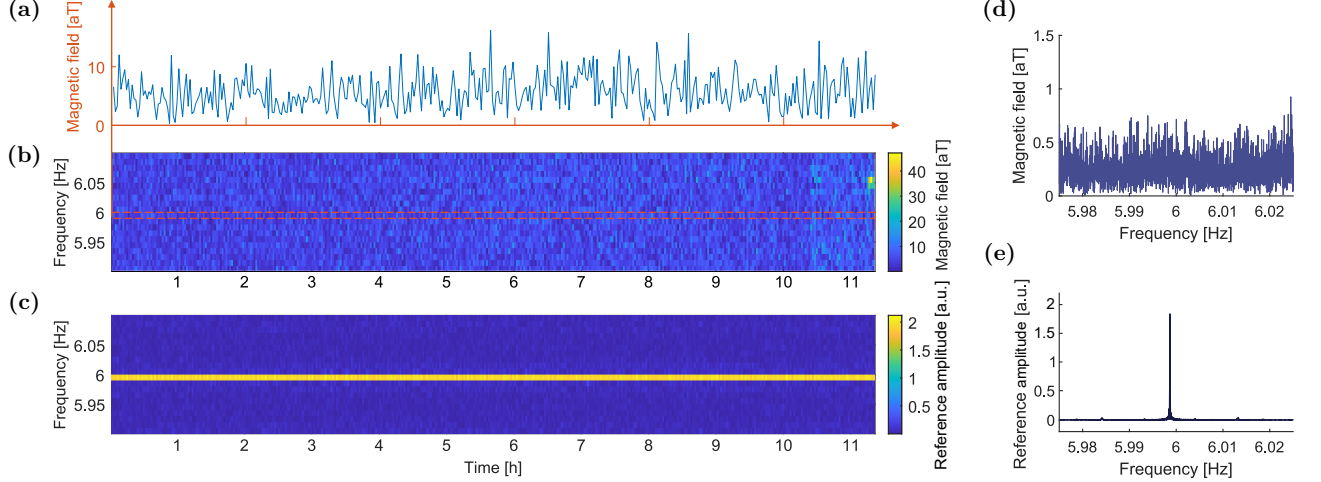


FIG. 3: Measured noise and corresponding signal frequency monitor. Magnetic noise at 6 Hz (a), spectrogram of the run (b), and of the reference signal (c), for the entire length of the measurement, divided in 72 seconds FFT. Both the spectra (d) and (e) are a single FFT of the whole run, showing the expected signal and the magnetic background. Plot (b) demonstrates that the system noise remains constant during the run, and that the pseudomagnetic field frequency is unaffected even by non-persistent magnetic bursts. The noise at the reference signal frequency is evidenced with an orange dashed line and reported in (a), showing that it is consistent with thermal fluctuations. The spectrogram (c) displays the reference signal, which is contained in a single bin for the whole length of the measurement, as demonstrated by (e).

noise (see Methods), or lowering the working temperature to also reduce the magnetisation fluctuations. While the latter upgrades basically improve the precision of the magnetometer, we envision an upscaling of the apparatus which simultaneously reduces the SQUID and magnetisation field noises, and increases the expected signal. The simplicity of the apparatus makes it easily scalable, and, as GSO is readily available in large quantities, we can use more than two parallel coils as pick-up and bolster the idea of the present scheme. An upgraded apparatus would allow us to use a large source which can increase the signal strength up to two orders of magnitude. For example, a setup with 50 cm-diameter source and a detector comprising 200 pick-up loops of 20 cm diameter, filled with GSO and read by a quantum-limited magnetometer, could in principle have the sensitivity to detect the model-predicted fifth force [10]. For what concerns the limitations of the scheme, we expect them to be related to technical noises rather than to fundamental issues. Spurious effects may show up when increasing the sensitivity, as for example the source masses'  $\chi$  modulating the Earth magnetic field, and mimicking the signal. We stress that a good magnetic screening is a key part of this setup, and of an upgraded one, as it must have the lowest noise and larger shielding factor.

## V. CONCLUSIONS AND OUTLOOK

In conclusion, we have designed and operated an experimental setup to search for spin-mass long-range forces

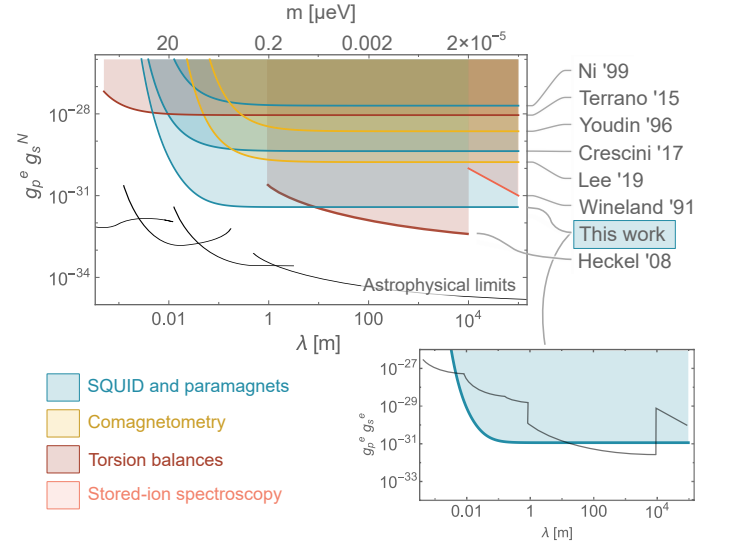


FIG. 4: Limits on spin mass interaction constants  $g_p^e g_s^N$  (upper) and  $g_p^e g_s^e$  (lower), derived from the present measurement and compared to the literature [12–24]. In the upper plot, the solid lines mark the experimentally excluded areas of the parameter space, and their color depends on the technique used for the measurement. The black lines are mixed laboratory and astrophysical constraints calculated by G. Raffelt [29]. In the lower plot, a solid blue line represent the result of this work, while the black line are the previous limits, obtained scaling the ones of the electron-nucleon interaction under the assumption that  $A = 2.5Z$  for all the source masses.

based on a SQUID-magnetometer with state-of-the-art sensitivity. Our search excludes the presence of pseudoscalar particles within a large region of the coupling-mass parameter space, which is of cosmological relevance for the physics case for axions and ALPs [8].

Thanks to this work, we believe that the combined advances related to an augmented and enhanced setup may lead to an unprecedented sensitivity level. Such setup will exclude or confirm the presence of pseudo-Goldstone bosons, like axions, predicted by current theories beyond the standard model, paving the way to a promising technique to search for the so-called “invisibles” particles in an extremely broad mass interval. Different experiments are searching for ALPs [37, 38] by exploiting the exceptional magnetic field sensitivity obtainable with SQUID-based magnetometers, and rapid progress can be foreseen in approaching problems like the study of magnetic noise [44] or the optimisation of the readout chain [36].

Eventually, we suggest that this kind of apparatus could be used for other fundamental searches, and may considerably improve existing results. The use of polarized sources [45] may extend the experimental sensitivity to the spin-spin interaction. As it does not violate parity and time reversal, its coupling constant is much larger than that for spin and mass, making it preferred for axion detection [27]. We finally mention that a closely similar, and possibly simpler, setup could be used to probe the gravitoelectromagnetic effects of Earth rotation on the elementary spin [46, 47], or the local presence of moving magnetic monopoles [48, 49].

### Acknowledgements

The authors want to acknowledge Mario Tessaro for his work on the superconducting wiring, on the electronics of the setup, and on the engine stabilization. We also thank Fulvio Calao and Enrico Berto for their help with the construction and test of the apparatus, and Ruggero Pengo for the advices on the cryogenics. The Cryogenic Service of the Laboratori Nazionali di Legnaro is acknowledged for providing us large quantities of liquid helium upon request. We deeply thank the AURIGA team for sharing their knowledge on mechanical and electromagnetic noise reduction. We also thank Yevgeny Stadnik for providing us with a theoretical point of view on the implications of these interactions. Eventually, we deeply acknowledge the Laboratori Nazionali di Legnaro for hosting and encouraging the experiment.

### Appendix A: Source and signal

The source masses are full lead cylinders enclosed into thin aluminium capsules, which are attached to the wheel. To put the masses in motion we use a high torque brushless motor phase-synchronized with a signal generator to precisely control the wheel rotational frequency.

The motor shaft and the wheel pivot are connected by two pulleys whose teeth number is such that the harmonics of the motor rotation does not fall on the signal frequency. This scheme ensures that the wheel’s rotational, and thus the signal’s, frequency is somewhat distanced from the motor’s own frequencies. Motor-related disturbances may be due to the specifics of the drive mechanism, and we verified that they are present in the broadband spectrum of the SQUID noise only if the motor is turned on. They are found not to influence the measurement noise. The masses are embedded in a low-density foam to avoid the effects of air-currents, and the whole wheel plus motor system was enclosed in a thin steel cage to reduce the air movement around the cryostat. Before starting the data acquisition, we initiate the wheel rotation and wait for some hours for the pulleys and motor to warm up in order to improve the frequency stability of the source. We monitor the signal frequency with a capacitive sensor coupled to the wheel, from which we record the pseudomagnetic field frequency for the whole run.

The displacement of the source masses creates the field modulation by changing  $r$ , the source-detector distance. For  $\lambda \ll r$  the potential in Eq. (2) is exponential. If  $\lambda \gg r$  it becomes a  $1/r^2$  potential, which produces a signal modulation independent on the mediator mass. This is similar to what is usually done in experiments testing gravity, which has a  $1/r$  potential with an infinite wavelength and no exponential decay. Our wheel and masses were designed to have a signal modulation of about a factor 2 for  $\lambda \simeq 10$  cm. without the need of a much larger apparatus. This choice makes it easier to screen the external disturbances like turbulences, vibrations and electromagnetic fields. A larger source would have been more space-consuming, had a larger inertia and an overall increased control complexity.

In the favoured case of the detection of a signal, this may be tested by lifting the cryostat to vary the source-detector distance, in order to estimate the range of the fifth force and hence the mass of the mediator. In our apparatus this modification is straightforward and does not require additional work on the setup.

Through a Fourier transform of the simulated signal we verified that the spectral leakage, i. e. the fraction of signal lost in the harmonics, is negligible for  $\lambda > 1$  cm, as our expected signal is much closer to a sine wave (no signal leakage) than to a square wave (significant signal leakage).

### Appendix B: Detector and readout

To match the  $1.8 \mu\text{H}$  input impedance of the SQUID we connect in parallel two pick-up inductances of roughly  $3.6 \mu\text{H}$ . The GSOs are housed in 3D-printed plastic supports, around which the pick-up coils are wound. Each inductance consists in 8 turns of NbTi wire distributed

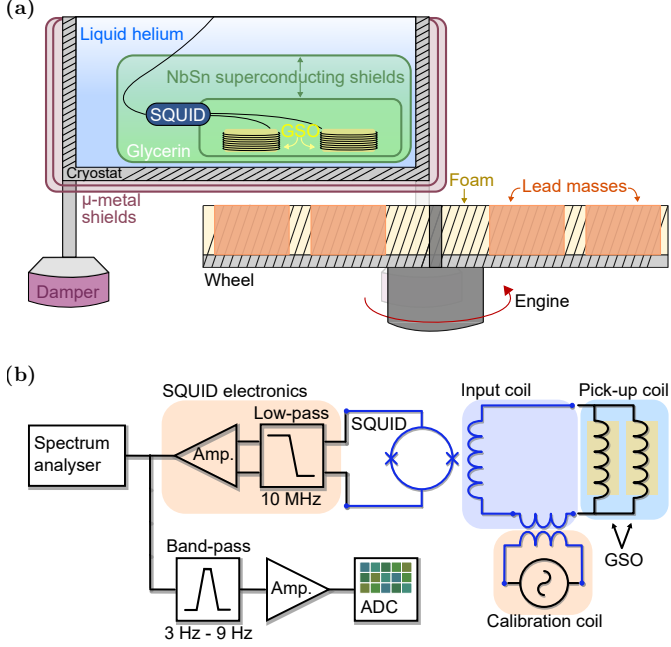


FIG. 5: **Section of the apparatus and detection circuit.** (a) Vertical section of the wheel, cryostat, and magnetic screens surrounding the detector. The drawing is not to scale. (b) Circuitual scheme of the detector. The blue circuits are printed on a board, while the black ones are external wires and electronics. The input and pick-up coils are framed in different colours as they are considered two single condensed element in the main text, and longer coil symbols correspond to larger inductances. The GSO crystals are shown as yellow rectangles, Amp. are the amplifiers, and ADC is an analog-to-digital converter.

over the height of the crystal. To design the pick-up, we tested the coil plus support system at liquid helium temperature, and verify the minimum dimensions which guarantee an adequate thermal stress resistance. The presence of the plastic supports increases the area of the coils with respect to that of the crystals'. We end up with a single coil surface of about  $\Sigma \simeq 11 \text{ cm}^2$  and correct our limit accordingly. Within the uncertainties, the calculated values of inductances and impedances are in good agreement with the measured values. The electronics of the SQUID system is reported in Fig. 5, which is a complete version of the simplified scheme in Fig. 2a.

The SQUID output is filtered and amplified before being split between two channels. The first is used as a monitor using a signal analyser, while the second is further filtered and amplified before being acquired by an analog-to-digital converter. The system is calibrated by the injection of a known current in a calibration coil (see Fig. 5), whose contribution to the inductance of the input coil is small. Subsequently, the field sensitivity of the detector is obtained considering the geometric features of the pick-up coil. The procedure's accuracy was tested in a previous work [22] with an additional calibration, namely the use of a large solenoid to provide a controlled and uniform AC field over the pick-up coil.

The two independent calibrations matched within experimental uncertainties, so for this work we relied on the reported one, and avoided the addition of other coils to the setup.

A spurious effect which mimics the pseudomagnetic signal is the modulation of the Earth's magnetic field related to the non-zero magnetic susceptibility of lead  $\chi_{\text{lead}} \simeq 10^{-5}$ ; in our setup this AC field is screened. However, exploiting this effect, we performed a consistency test based on standard electromagnetism to further enforce our result. A 30 cm-diameter coil made of a copper wire is used to produce a static field. It is placed below the rotating wheel and parallel to it, to put the source masses in a field of  $\sim 1 \text{ mT}$ . With respect to the Earth magnetic field, this one increases the magnetic signal modulated by the rotation of the masses and generated by  $\chi_{\text{lead}}$ . Despite having a  $1/r$  potential, we use the resulting AC field to simulate the pseudomagnetic signal, to confirm its frequency and, to some extent, test the setup magnetic sensitivity. A precise investigation is not possible as the static field also degrades the magnetic shielding, and as the SQUID noise results slightly higher when it is turned on, possibly due to fluctuations in the static field amplitude. Moreover, other effects may be competing with this one, as e.g. the field modulation related to the skin effect in the lead masses.

### Appendix C: Background estimation and signal analysis

The SQUID noise at the pick-up depends on the inductances of the input coil, of the pick-up coil and on the mutual inductance between the input coil and the SQUID loop  $M_i$ . The flux power spectral density of the intrinsic detector noise at  $L_p$  can be calculated as [34]

$$S_{\phi}^{(p)}(\omega) = \frac{(L_p + L_i)^2}{M_i^2} S_{\phi}(\omega). \quad (\text{C1})$$

The magnetic field noise can be calculated from Eq. (C1) as  $S_B^{(p)}(\omega)^{1/2} = S_{\phi}^{(p)}(\omega)^{1/2} / N_p n_p \Sigma$ , where  $N_p = 2$  is the number of pick-up coils and  $n_p = 8$  is the number of turns of area  $\Sigma$  forming each coil. Our sensor has a flux noise per unit of bandwidth  $S_{\phi}(\omega)^{1/2} \simeq 1 \mu\phi_0 / \sqrt{\text{Hz}}$ , input and pick-up inductances  $L_i \simeq L_p \simeq 1.8 \mu\text{H}$ , and SQUID- $L_i$  mutual inductance  $M_i \simeq 8.8 \text{ nH}$ , leading to an expected field noise  $S_B^{(p)}(\omega)^{1/2} = 46 \text{ aT} / \sqrt{\text{Hz}}$ , which is in agreement with the measured background. The energy resolution of our system may be calculated as

$$\epsilon = \frac{1}{2} L_i S_{\phi}(\omega) / M_i^2 = 443 \hbar \quad (\text{C2})$$

meaning that a quantum limited SQUID sensor, with  $1 \hbar$  energy resolution, could improve the present magnetic field sensitivity of a factor  $\sqrt{\epsilon/\hbar} \simeq 20$ .

The magnetisation noise is expected to contribute to the noise budget of the experiment, and its magnitude

can be quantified using the fluctuation-dissipation theorem as

$$S_M^{(p)}(\omega)^{1/2} = \sqrt{\frac{2k_B T}{\pi\mu_0} \frac{\chi\tau}{V}}, \quad (\text{C3})$$

where  $V \simeq 14 \text{ cm}^3$  is the crystals' volume, and  $\tau \simeq 70 \text{ ps}$  is the spin relaxation time of the GSO, measured at 80 K through an electron paramagnetic resonance [39, 40]. With our experimental parameters the magnetisation noise results  $12 \text{ aT}/\sqrt{\text{Hz}}$ , which is compatible with the added noise present in our spectra. We tested the system with and without GSO crystals inserted. However, to satisfy the matching condition  $L_p \simeq L_i$  in the two configurations, the number of turns of the coils have to be changed in order to compensate the higher inductance related to the crystals' magnetic susceptibility. This adds a systematic uncertainty in the comparison of the two measurements, which is difficult to take into account, and prevents us from reporting a differential result. Referring to Fig. 2d, we consider a frequency interval close to the pseudomagnetic signal frequency, to estimate the uncertainty of the measured noise level.

In a complementary way, the noise spectra presented in Fig. 2d and in Fig. 3 demonstrate the absence of a persistent signal in our data set. The former shows that with the minimum bandwidth allowed by the experimental integration time there is no trace of a signal, while the latter ensures the stability of the measurement throughout the run. The small field excess in Fig. 2d at 6.05 Hz is justified by the data in Fig. 3b, which also displays that this increase is not persistent, is not at the pseudomagnetic field frequency, and is not contained within one frequency bin. We conclude that it can not be confused with a signal.

#### Appendix D: Spurious noise reduction

In this experimental scheme the working frequency can be precisely managed by varying  $f_w$ , which is a major advantage in the control and reduction of the external noises. The nature of these disturbances is usually electromagnetic or mechanical; hereafter we list the different

measures we took to reduce such effects.

Electromagnetic disturbances are related to the environment and to the instruments used in the experiment, like the motor driving the wheel. As shown in Fig. 5a, the design of our apparatus was optimised to get the minimum source-detector distance while preserving a satisfactory screening of the magnetometer. The details of the magnetic shields are as follows. Two  $\mu$ -metal cans are placed around the cryostat at room temperature. Two superconducting shields are immersed in liquid helium, one comprises a large volume around the detector and the second only contains the crystals and pick-up coils. These cryogenic shields are made of single lead-tin sheets, with no soldered joints. A third shield is dedicated to the SQUID chip, and is made of niobium. Besides the magnetic screening, the  $\mu$ -metal is useful to allow the superconducting transition of the screens to occur in a reduced static magnetic field, improving their rejection factor. Considerable effort was made to eliminate possible electromagnetic cross-talk between the power electronics of the motor and the magnetometer, and for the same reason the square wave reference signal given by the capacitive sensor of the source is smoothed with a low-pass filter. Some other techniques that we used to avoid the presence of spurious signals at the pseudomagnetic field frequency were presented in the description of the source system.

Mechanical vibrations are driven by the wheel rotation, and by the external environment, so, to reduce them, we isolate the cryostat from the source and from the surroundings. The cryostat was decoupled from the ground with four legs resting on alternate layers of lead and Sylodamp<sup>®</sup> SP1000, a polyurethane elastomer which damps vibrations. Turbulences and acoustic disturbances related to the masses rotation are diminished thanks to the geometry of the source, which is made as uniform as possible, and by enclosing the motor plus wheel system in a thin aluminium cage. A relative movement between the detector and the static field trapped in the superconducting shields is particularly problematic, as it leads to a magnetic flux in the pick-up coils. To drastically reduce this issue we fill the chamber containing the screens and the coils with glycerin, which freezes at low temperature and blocks all the relative vibrations.

- 
- [1] Alessandro Bettini. *Introduction to Elementary Particle Physics*. Cambridge University Press, 2008.
  - [2] David Griffiths. *Introduction to Elementary Particles*. John Wiley & Sons, Ltd, 2008.
  - [3] Richard P. Feynman, Fernando B. Morinigo, and William G. Wagner. Feynman lectures on gravitation. *European Journal of Physics*, 24(3):330–330, may 2003.
  - [4] Michael. J. Duff. M-theory (the theory formerly known as strings). *International Journal of Modern Physics A*, 11(32):5623–5641, 1996.
  - [5] Steven Weinberg. Approximate symmetries and pseudo-goldstone bosons. *Phys. Rev. Lett.*, 29:1698–1701, Dec 1972.
  - [6] Roberto D. Peccei and Helen R. Quinn. CP conservation in the presence of pseudoparticles. *Phys. Rev. Lett.*, 38:1440–1443, Jun 1977.
  - [7] Steven Weinberg. A new light boson? *Phys. Rev. Lett.*, 40(4):223, 1978.
  - [8] David J.E. Marsh. Axion cosmology. *Physics Reports*, 643:1 – 79, 2016. Axion cosmology.
  - [9] Joerg Jaeckel and Andreas Ringwald. The Low-Energy Frontier of Particle Physics. *Ann. Rev. Nucl. Part. Sci.*,



- 60:405–437, 2010.
- [10] Igor G. Irastorza and Javier Redondo. New experimental approaches in the search for axion-like particles. *Progress in Particle and Nuclear Physics*, 102:89 – 159, 2018.
  - [11] J. E. Moody and Frank Wilczek. New macroscopic forces? *Phys. Rev. D*, 30:130–138, Jul 1984.
  - [12] P.V. Vorobyov and Ya.I. Gitarts. A new limit on the arion interaction constant. *Physics Letters B*, 208(1):146 – 148, 1988.
  - [13] D. J. Wineland, J. J. Bollinger, D. J. Heinzen, W. M. Itano, and M. G. Raizen. Search for anomalous spin-dependent forces using stored-ion spectroscopy. *Phys. Rev. Lett.*, 67:1735–1738, Sep 1991.
  - [14] B. J. Venema, P. K. Majumder, S. K. Lamoreaux, B. R. Heckel, and E. N. Fortson. Search for a coupling of the earth’s gravitational field to nuclear spins in atomic mercury. *Phys. Rev. Lett.*, 68:135–138, Jan 1992.
  - [15] R. C. Ritter, L. I. Winkler, and G. T. Gillies. Search for anomalous spin-dependent forces with a polarized-mass torsion pendulum. *Phys. Rev. Lett.*, 70:701–704, Feb 1993.
  - [16] A. N. Youdin, D. Krause, Jr., K. Jagannathan, L. R. Hunter, and S. K. Lamoreaux. Limits on spin-mass couplings within the axion window. *Phys. Rev. Lett.*, 77:2170–2173, Sep 1996.
  - [17] Wei-Tou Ni, Sheau-shi Pan, Hsien-Chi Yeh, Li-Shing Hou, and Juling Wan. Search for an axionlike spin coupling using a paramagnetic salt with a dc squid. *Phys. Rev. Lett.*, 82:2439–2442, Mar 1999.
  - [18] Giles D. Hammond, Clive C. Speake, Christian Trenkel, and Antonio Pulido Patón. New constraints on short-range forces coupling mass to intrinsic spin. *Phys. Rev. Lett.*, 98:081101, Feb 2007.
  - [19] B. R. Heckel, E. G. Adelberger, C. E. Cramer, T. S. Cook, S. Schlamminger, and U. Schmidt. Preferred-frame and  $cp$ -violation tests with polarized electrons. *Phys. Rev. D*, 78:092006, Nov 2008.
  - [20] S. A. Hoedl, F. Fleischer, E. G. Adelberger, and B. R. Heckel. Improved constraints on an axion-mediated force. *Phys. Rev. Lett.*, 106:041801, Jan 2011.
  - [21] W. A. Terrano, E. G. Adelberger, J. G. Lee, and B. R. Heckel. Short-range, spin-dependent interactions of electrons: A probe for exotic pseudo-goldstone bosons. *Phys. Rev. Lett.*, 115:201801, Nov 2015.
  - [22] N. Crescini, C. Braggio, G. Carugno, P. Falferi, A. Ortolan, and G. Ruoso. Improved constraints on monopole-dipole interaction mediated by pseudo-scalar bosons. *Physics Letters B*, 773:677 – 680, 2017.
  - [23] Xing Rong, Mengqi Wang, Jianpei Geng, Xi Qin, Maosen Guo, Man Jiao, Yijin Xie, Pengfei Wang, Pu Huang, Fazhan Shi, Yi-Fu Cai, Chongwen Zou, and Jiangfeng Du. Searching for an exotic spin-dependent interaction with a single electron-spin quantum sensor. *Nature Communications*, 9(1):739, Feb 2018.
  - [24] Junyi Lee, Attaallah Almasi, and Michael Romalis. Improved limits on spin-mass interactions. *Phys. Rev. Lett.*, 120:161801, Apr 2018.
  - [25] Geoff Brumfiel. The waiting game. *Nature*, 429(6987):10–11, May 2004.
  - [26] P.-H. Chu, E. Weisman, C.-Y. Liu, and J. C. Long. Search for exotic short-range interactions using paramagnetic insulators. *Phys. Rev. D*, 91:102006, May 2015.
  - [27] Asimina Arvanitaki and Andrew A. Geraci. Resonantly detecting axion-mediated forces with nuclear magnetic resonance. *Phys. Rev. Lett.*, 113:161801, Oct 2014.
  - [28] Lei Chen, Jian Liu, and Kadi Zhu. Ultrasensitive optomechanical detection of an axion-mediated force based on a sharp peak emerging in probe absorption spectrum, 2019.
  - [29] Georg Raffelt. Limits on a  $cp$ -violating scalar axion-nucleon interaction. *Phys. Rev. D*, 86:015001, Jul 2012.
  - [30] Y. V. Stadnik, V. A. Dzuba, and V. V. Flambaum. Improved limits on axionlike-particle-mediated  $p$ ,  $t$ -violating interactions between electrons and nucleons from electric dipole moments of atoms and molecules. *Phys. Rev. Lett.*, 120:013202, Jan 2018.
  - [31] Pavel Fadeev, Yevgeny V. Stadnik, Filip Ficek, Mikhail G. Kozlov, Victor V. Flambaum, and Dmitry Budker. Revisiting spin-dependent forces mediated by new bosons: Potentials in the coordinate-space representation for macroscopic- and atomic-scale experiments. *Phys. Rev. A*, 99:022113, Feb 2019.
  - [32] T. M. Leslie, E. Weisman, R. Khatriwada, and J. C. Long. Prospects for electron spin-dependent short-range force experiments with rare earth iron garnet test masses. *Phys. Rev. D*, 89:114022, Jun 2014.
  - [33] Lev D. Landau and Evgenij M. Lifshitz. *Theoretical Physics IX - Statistical physics II: theory of the condensed state*. Editori riuniti - university press, 2010.
  - [34] John Clarke and Alex I. Braginski, editors. *The SQUID Handbook: Fundamentals and Technology of SQUIDS and SQUID Systems*. Wiley-VCH, 2005.
  - [35] J. E. Zimmerman. Sensitivity enhancement of superconducting quantum interference devices through the use of fractional-turn loops. *Journal of Applied Physics*, 42(11):4483–4487, 1971.
  - [36] Jan-Hendrik Storm, Peter Hömmen, Dietmar Drung, and Rainer Körber. An ultra-sensitive and wideband magnetometer based on a superconducting quantum interference device. *Applied Physics Letters*, 110(7):072603, 2017.
  - [37] Jonathan L. Ouellet, Chiara P. Salemi, Joshua W. Foster, Reyco Henning, Zachary Bogorad, Janet M. Conrad, Joseph A. Formaggio, Yonatan Kahn, Joe Minervini, Alexey Radovinsky, Nicholas L. Rodd, Benjamin R. Safdi, Jesse Thaler, Daniel Winklehner, and Lindley Winslow. First results from abracadabra-10 cm: A search for sub- $\mu$ eV axion dark matter. *Phys. Rev. Lett.*, 122:121802, Mar 2019.
  - [38] Alexander V. Gramolin, Deniz Aybas, Dorian Johnson, Janos Adam, and Alexander O. Sushkov. Search for axion-like dark matter with ferromagnets. *Nature Physics*, Aug 2020.
  - [39] B. Baiboussinov, C. Braggio, A. Cardini, G. Carugno, F. Congiu, S. Gain, G. Galeazzi, A. Lai, A. Lehman, P. Mocchi, A. Mura, F. Quochi, M. Saba, B. Saitta, and G. Sartori. An active electron polarized scintillating GSO target for neutrino physics. *Nuclear Instruments and Methods in Physics Research A*, 694:335–340, December 2012.
  - [40] N. Crescini, C. Braggio, G. Carugno, P. Falferi, A. Ortolan, and G. Ruoso. The quax-gpgs experiment to search for monopole-dipole axion interaction. *Nuclear Instruments and Methods in Physics Research Section A: Accelerators, Spectrometers, Detectors and Associated Equipment*, 842:109 – 113, 2017.
  - [41] Andrea Vinante, Renato Mezzena, Giovanni Andrea Prodi, Stefano Vitale, Massimo Cerdonio, Paolo Falferi,

- and Michele Bonaldi. Dc superconducting quantum interference device amplifier for gravitational wave detectors with a true noise temperature of  $16\ \mu\text{k}$ . *Applied Physics Letters*, 79(16):2597–2599, 2001.
- [42] Andrea Vinante. *Optimization of a Two-Stage dc SQUID for Resonant Gravitational Wave Detectors*. PhD thesis, Trento U., 2002.
- [43] P. Falferi, M. Cerdonio, L. Franceschini, R. Macchietto, S. Vitale, and J. P. Zendri. A high inductance khz resonator with a quality factor larger than  $10^6$ . *Review of Scientific Instruments*, 65(9):2916–2919, 1994.
- [44] Jukka Nenonen, Juha Montonen, and Toiro Katila. Thermal noise in biomagnetic measurements. *Review of Scientific Instruments*, 67(6):2397–2405, 1996.
- [45] G. D. Hammond, A. Pulido Patón, C. C. Speake, C. Trenkel, G. K. Rochester, D. Shaul, and T. J. Sumner. New spin source to search for scalar-pseudoscalar couplings at short range. *Phys. Rev. D*, 77:036005, Feb 2008.
- [46] Bahram Mashhoon. Can einstein’s theory of gravitation be tested beyond the geometrical optics limit? *Nature*, 250(5464):316–317, Jul 1974.
- [47] Bahram Mashhoon. Gravitational couplings of intrinsic spin. *Classical and Quantum Gravity*, 17(12):2399–2409, jun 2000.
- [48] Blas Cabrera. First results from a superconductive detector for moving magnetic monopoles. *Phys. Rev. Lett.*, 48:1378–1381, May 1982.
- [49] Ritika Dusad, Franziska K. K. Kirschner, Jesse C. Hoke, Benjamin R. Roberts, Anna Eyal, Felix Flicker, Graeme M. Luke, Stephen J. Blundell, and J. C. Séamus Davis. Magnetic monopole noise. *Nature*, 571(7764):234–239, Jul 2019.